JOURNAL OF THERMOPLASTIC COMPOSITE MATERIALS

Original research article

Magnetically responsive PVA/Fe_3O_4 nanofibers: Fabrication and characterization for potential applications in stimuli-responsive systems

Journal of Thermoplastic Composite Materials
2026, Vol. 0(0) 1–25

DOI: 10.1177/08927057261424773
journals.sagepub.com/home/jtc
Sage

Anderson Fernández[1], Omar D. Gutiérrez[1], Tiffany Marin[1] and Oscar Arnache[2]

Abstract

Stimuli-responsive nanocomposite systems have emerged as promising platforms for the development of externally actuated devices in both biomedical and environmental applications. In this study, polyvinyl alcohol (PVA)/magnetite nanoparticle (MNP) nanocomposite fibers were successfully fabricated via electrospinning. Magnetite nanoparticles were synthesized electrochemically at room temperature using a non-toxic electrolyte, thereby supporting an environmentally sustainable approach. Structural and magnetic characterization confirmed the formation of the magnetite (Fe_3O_4) phase, with particle sizes predominantly in the 12–20 nm range and a saturation magnetization value of 79.3 emu/g. The incorporation of MNPs into the PVA matrix yielded uniform fibers with a 27% increase in average diameter, as confirmed by SEM–EDX. FTIR analyses demonstrated that the polymer's chemical structure remained unchanged and nanoparticle oxidation was minimal, preserving magnetic functionality. The PVA/MNP nanocomposites were evaluated in a diffusion cell containing an acetaminophen solution for 3.5 h, using a permanent magnet with a field strength of 0.5 T (Tesla) as a remote-control stimulus, resulting in a control of diffused 35 %. The nanocomposites exhibited magnetically triggered drug release behavior, indicating their potential for application in controlled

[1]Grupo Química Básica, Aplicada y Ambiente – Alquimia, Facultad de Ciencias Exactas y Aplicadas, Instituto Tecnológico Metropolitano, Medellín, Colombia
[2]Grupo de Estado Sólido, Instituto de Física, Universidad de Antioquia, Medellín, Colombia

Corresponding author:
Tiffany Marin, Grupo Química Básica, Aplicada y Ambiente – Alquimia, Facultad de Ciencias Exactas y Aplicadas, Instituto Tecnológico Metropolitano, Calle 73 #76A – 354, Medellín 050034, Colombia.
Email: tiffanymarin@itm.edu.co

release systems with external control of formulation. These findings establish PVA/MNP nanocomposites as viable candidates for magnetically stimuli-responsive systems.

Keywords
Nanocomposite fibers, magnetite nanoparticles, electrochemical synthesis, electrospinning techniques, stimuli-responsive systems

Introduction

Nanotechnology has revolutionized scientific research across various fields by exploiting of the unique properties that materials exhibit at the nanometer scale, which are significantly different from those of their macroscopic counterparts.[1–3] In particular, biomedical applications have increasingly focused on the development of nanocomposites for drug delivery, controlled release,[4–6] cellular regeneration[7,8] and biosensors.[9] Nanoscale polymer systems, when fabricated as nanocomposite structures, can be engineered to respond to specific chemical, physical, and biochemical triggers. These stimuli may include changes in temperature, pH, ionic strength, exposure to electromagnetic radiation or ultrasound, redox potential, electric current, enzyme or protein activity, and magnetic fields.[10–12]

One of the most widely used materials for these applications is magnetite nanoparticles, which stand out among other nanomaterials, such as silver, gold, titanium, and aluminum due to their magnetic properties, high surface-to-volume ratio, antimicrobial activity, and inherent biocompatibility.[13,14] These characteristics enable their use in a wide range of biomedical applications, including controlled drug delivery, hyperthermia, magnetic resonance imaging contrast, and the fabrication of scaffolds for cell regeneration. Moreover, magnetic nanoparticles serve as a versatile platforms for the simultaneous diagnosis and treatment of cancer, as well as for Fenton-type catalytic activity.[15–17] Given the properties exhibited by magnetite nanoparticles, various synthesis methods have been developed to optimize both production processes and the physical and chemical characteristics of the nanoparticles.[18,19] Hence, the most commonly reported methods for the synthesis of MNPs include co-precipitation, thermal decomposition, sol–gel and electrochemical synthesis.[20–22] Electrochemical synthesis enables precise control over the diameter and morphology of the nanoparticles (MNPs) by modulating variables such as cell geometry, applied voltage, current density, electrolyte type, and the distance between the electrodes.[23,24] This method allows for the production of MNPs with low polydispersity and eliminates the use of harmful chemicals, such as NaOH, as well as the high temperatures associated with other methods.[7,24,25] Research on the electrochemical synthesis of MNPs has shown that the nanoparticles can be produced using relatively accessible precursors, such as NaCl or KCl based electrolyte solutions and iron electrodes, which supply Fe^{2+} and Fe^{3+} ions.[23,24,26] These investigations report the production of MNPs with low polydispersity, tunable particle sizes, superparamagnetic behavior, and the ease of scaling up the electrochemical process. Overall, this approach represents a

safe, reliable, and efficient alternative that does not compromise the quality and functionality of the MNPs.[23,27,28]

Recent studies have focused on incorporating MNPs into various biocompatible polymeric matrices, such as polyvinyl alcohol, collagen, chitosan, polycaprolactone (PCL), and cellulose, by taking advantage of the synergy between the two materials to development of devices that respond to external magnetic stimuli.[29–33] Polyvinyl alcohol (PVA) has stood out due to its thermal stability, excellent biocompatibility, and high mechanical performance. In addition, it is considered a smart polymer material, and several studies have investigated its properties as a shape memory polymer (SMP).[34] These properties enable the use of the polymeric material in the manufacture of various biomedical devices, such as drug delivery systems and scaffolds for cell regeneration.[10,35,36] Currently, different methods for integrating both materials are being investigated, with electrospinning proving to be an ideal technique for this purpose.[37,38] The electrospinning technique has proven particularly effective in integrating both materials, producing PVA/MNPs fibers with morphological characteristics similar to those of the extracellular environment. These fibers also exhibit a high surface to volume ratio and can be stimulated by magnetic fields.[39] The developed nanocomposites exhibit a set of highly promising properties for medical applications, including exceptional antimicrobial activity, which makes them suitable for the fabrication of dermal dressings.[40] Their morphological structure, which closely resembles the extracellular environment, enables them to serve as support for cell growth and proliferation.[32] Furthermore, they function as drug delivery systems, making them suitable platforms for the controlled release of therapeutic agents.[41,42] Recently, these systems have been recognized as effective platforms for the diagnosis and treatment of various diseases, particularly in biosensor applications.[13,32,43]

In 2016, Cai and his collaborators[44] integrated MNPs into chitosan and gelatin membranes using the electrospinning technique. They found that the presence of nanoparticles (NPs) inhibited the growth of bacteria such as Staphylococcus aureus, paving the way for development of dressings based on these materials. In 2021, Funnell and collaborators[39] investigated the effect of magnetic fields on neurite outgrowth in electrospun scaffolds embedded with MNPs, observing a 40% increase in neuronal protrusion growth under the influence of a magnetic field compared to the control system. Similarly, Perera and collaborators[45] electrospun PVA membranes with embedded MNPs for use in drug release systems based on a dissolution mechanism. The researchers found that the membranes dissolved more rapidly under the action of the magnetic field, resulting in faster drug release compared to the system without NPs. The properties exhibited by PVA/MNPs fibers have facilitated the continued development of controlled drug-release systems. These release methods have proven to be potentially effective for transdermal drug delivery, acting as diffusion barriers between the drug reservoir and the stratum corneum of the skin. This approach enables tropical drug administration and offers the possibility of controlled release through magnetic stimulation.[46,47] However, despite existing studies linking the properties of MNPs incorporated into polymeric systems with their response to external magnetic fields, there remains a notable lack of information in the literature regarding the electrochemical production of MNPs and their

subsequent incorporation into polymeric matrices via electrospinning for the development of nanocomposites. This study presents the development of PVA/MNP nanocomposites via the electrochemical synthesis of magnetite nanoparticles, a technique that offers advantages such as controlled size distribution and morphology, room temperature operation, and the use of water as a solvent. The MNPs are subsequently integrated into a PVA polymer matrix via dispersion without surface modification, and fibers are formed using the electrospinning technique. Furthermore, the physicochemical properties of the MNPs are characterized, and the nanocomposite response to external magnetic stimuli is demonstrated, highlighting its potential as a stimulus-responsive system.

Materials and Methods

Materials

The synthesis of nanocomposite fibers was made using: absolute ethanol (96%) and sodium chloride (NaCl) were purchased from Merck®. A low-carbon steel bar (AISI-SAE 1006) with mass composition (%) 0.042 C, 0.006 Si, 0.027 P, 0.034 S, 0.0359 Mn, 0.012 Cr, 0.006 Mo, 0.027 Cu, 0.035 Ni and 99.45. Fe was employed as an anode, while a cylindrical AISI 304 stainless steel mesh, composed of an Fe-based alloy containing approximately 18% chromium and 10% nickel (Fe/Cr 18%/Ni 10%), was used as the cathode. The stainless steel mesh was commercially purchased from Merck. Additionally, commercial polyvinyl alcohol (94%, Mw = 31.000 – 50.000 Da, 88% hydrolyzed from Protokimica®) was employed as the polymeric matrix. Acetaminophen (GR) was purchased from Sigma-Aldrich.

Synthesis of magnetite nanoparticles (MNPs)

The MNPs were obtained through electro-oxidation in an electrochemical cell with a concentric arrangement for electrodes, following the methodology described by Marin and collaborators.[24] A low-carbon steel bar was used as the anode and iron precursor (Fe^{2+}; Fe^{3+}), while a cylindrical stainless-steel mesh (304) surrounding the anode served as the cathode. During the synthesis, the electrodes were maintained at a distance of no more than 1 cm and were connected to a DC BK PRESICION model 1671-A power supply, which allowed for the control of the current density at 100 mA/cm^2 for 10 minutes. A 0.05 M NaCl solution in a 50% v/v (water/ethanol mixture) was used as the electrolyte and dispersant medium for the newly formed magnetite nanoparticles. The electrochemical cell was submerged in an ultrasound bath (Elmasonic EASY 30 H) operating at 60 Hz during the synthesis. Subsequently, the synthesized MNPs were washed and centrifuged to remove most of the electrolyte. Finally, the nanoparticles were stored in an inert $N_{2(g)}$ atmosphere and dried at 40°C for 24 h.

Fabrication of nanocomposite fibers

The PVA/MNPs solution was prepared by dissolving 1.20 g of PVA in 10.0 mL of deionized water under constant stirring and heating at 60°C for 3.0 h. Once the mixture reached room temperature and the polymer was fully dissolved, 0.12 g of MNPs were added and subsequently dispersed by bath sonication, operating at 60 Hz, for 15 min in 5-min cycles each. The PVA/MNPs nanocomposite fibers were obtained using the Fluidnatek® model LE-100 electrospinning unit, equipped with a fixed flat collector plate and vertically arranged needle. The operating parameters used for fiber formation were a needle-to-collector distance of 10 cm, a flow rate of 0.5 mL/h, and a voltage of 18 kV applied to the needle and −1 kV to the collector plate. For the electrospinning process, a needle with an inner diameter of 1.19 mm and an outer diameter of 1.65 mm was used. The spinning time for forming each PVA and PVA/MNPs membranes was 3 h (See Figure 1).

Characterization

The size distribution and morphology of the nanoparticles were studied using Transmission Electron Microscopy (TEM) with the Tecnai F20 Super Twin TMP de FEI. Their composition of NPs was determined by Raman spectroscopy using the Raman microspectrometer Horiba Jobin Yvon®, model HR 800 equipped with a D2 filter, a 633 nm laser, and a power of 0.106 mW over three cycles, using a DU420A-EO-325 detector (Horiba®). The crystalline structure of the synthesized nanoparticles was analyzed through the Selected Area Electron Diffraction (SAED) pattern and HR-TEM micrographs obtained by TEM. In addition, the X-Ray Diffraction (XRD) pattern was obtained using an Empyrean (PANalytical®) with Cu Kα, performing measures from 8° to 85° 2θ at a scan rate of 0.026°/s with a step time of 50 s. The chemical structure of the fibers was

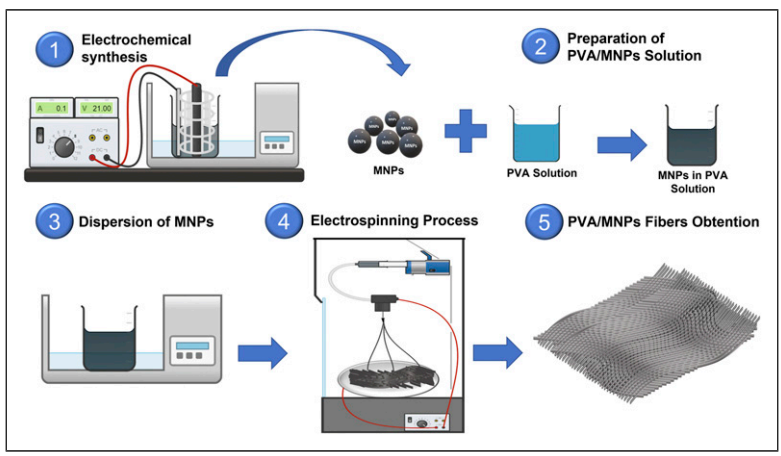

Figure 1. Schematic representation PVA/MNPs nanocomposite fibers of the production process.

studied through Fourier Transform Infrared (FTIR) spectroscopy using a SHIMADZU® IRTrace-100 spectrometer, equipped with an attenuated total reflection (ATR) accessory, a resolution of 4 cm^{-1} and scans over a range of 600 to 4200 cm^{-1}. The size distribution and morphology of the nanocomposite fibers were characterized by Scanning Electron Microscopy (SEM) micrographs and Energy Dispersing X-Ray spectroscopy (EDS) images, obtained using a JEOL® JSM-7100 Field Emission Gun (FEG) SEM. Finally, the magnetic properties of the magnetite nanoparticles were assessed through magnetic measurements using a Physical Property Measurement System (PPMS, Quantum Design) and a vibrating-sample magnetometer (VSM).

Release profile test by diffusion experiments

The drug release experiment was conducted using a diffusion cell, with acetaminophen employed as a model drug. The diffusion cell was separated in two compartments (L1 and L2) by an electrospun membrane. Two types of electrospun membranes were evaluated: PVA and PVA/MNPs. During each experiment, 500 mL of a 1000 ppm acetaminophen solution was added to compartment L1, while 500 mL of deionized water was added to compartment L2. The PVA and PVA/MNPs membranes were evaluated both in the absence of a magnetic field and under the application of a 0.5 T magnetic field using a neodymium magnet (N50 grade). Each type of experiment was performed in triplicate for all membranes. Aliquots were collected from the diffusion cell at 0, 30, 60, 90, 120, 150, 180, and 210 min, with 5.0 mL samples withdrawn from compartment L2. Each sample was analyzed using a Cary Spectrophotometer UV-VIS spectrophotometer (Varian®) at a wavelength of 243 nm, corresponding to the maximum characteristic absorbance of acetaminophen.[45]

Results and Discussion

Characterization of iron oxide particles

The iron oxide formed during the synthesis changed the color of the electrolyte, passing through yellow to dark yellow and finally black. According to published works on electrochemical synthesis of MNPs, the variation in the color of the electrolyte represents the successive appearance of different phases of various iron oxide-hydroxides that form until the magnetite phase is reached. Therefore, the chemical species attributed precursors of magnetite (Fe_3O_4) were Iron Hydroxide $Fe(OH)_2$, Green Rust $Fe^{II}{}_3Fe^{III}(OH)_8Cl.2H_2O$ (Chlorides from the NaCl), and Lepidocrocite (ɣ-FeOOH).[23,48,49] The following sections present the analysis of size distribution, chemical composition, and crystal structure of iron oxide obtained in this work.

Analysis of morphology and size of iron oxide particles. The size distribution and morphology are shown in Figure 2. The measurements were conducted by assessing the distance between the most equidistant points of the particle's shape. No predefined geometric

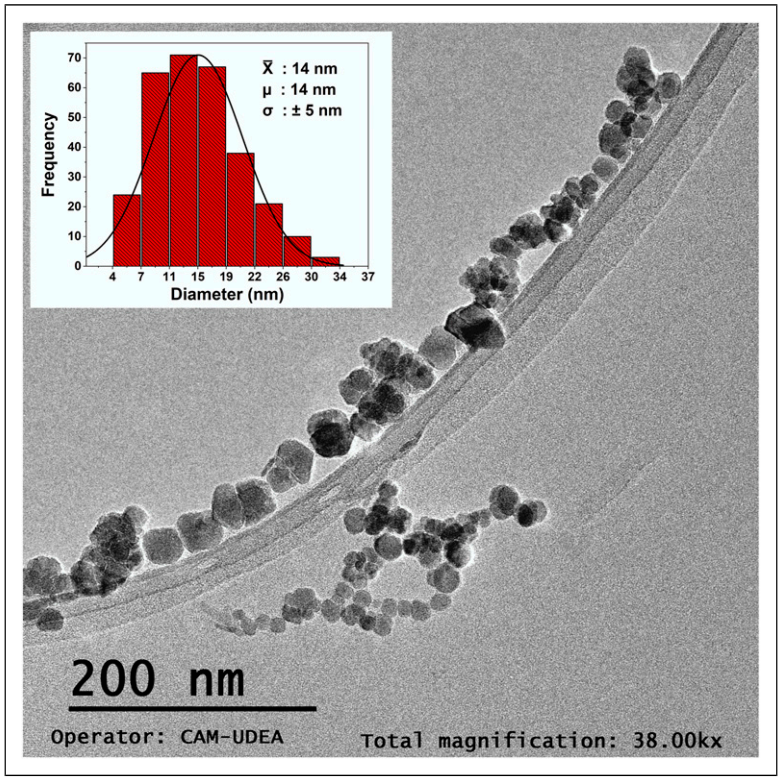

Figure 2. TEM micrograph of MNPs obtained by electrochemical synthesis, morphologic and size distribution histogram (n = 280, by triplicate).

models were applied to measure the nanoparticles. The data were grouped to generate the corresponding histogram (see inset of Figure 2).

The average particle size was 14 nm, with a median of 14 nm and a standard deviation of 5 nm. It was observed that the size distribution of nanoparticles follows a Gaussian trend, as shown in the histogram, with an R^2 value of 0.92. This suggests that the Gaussian model used to describe the particle size distribution provides a good approximation. Additionally, it was found that more than 85% of the nanoparticles are below 20 nm, which provides an initial indication of potential superparamagnetic behavior.[50,51]

Analysis of the chemical composition of nanoparticles. The magnetite phase was identified using Raman spectroscopy. Figure 3 presents the spectrum obtained for the synthesized nanoparticles, where the band at 670 cm^{-1}, attributed to the A_{1g} transition, facilitates the identification of one of the characteristic vibrational modes of this oxide.[52] This band corresponds to the symmetrical vibrations of the Fe-O bonds of the inverse spinel crystalline structure of magnetite, serving as a clear indication of the presence of this phase.[53–55] Additionally, the presence of bands in the regions 541-556 cm^{-1} and 305-

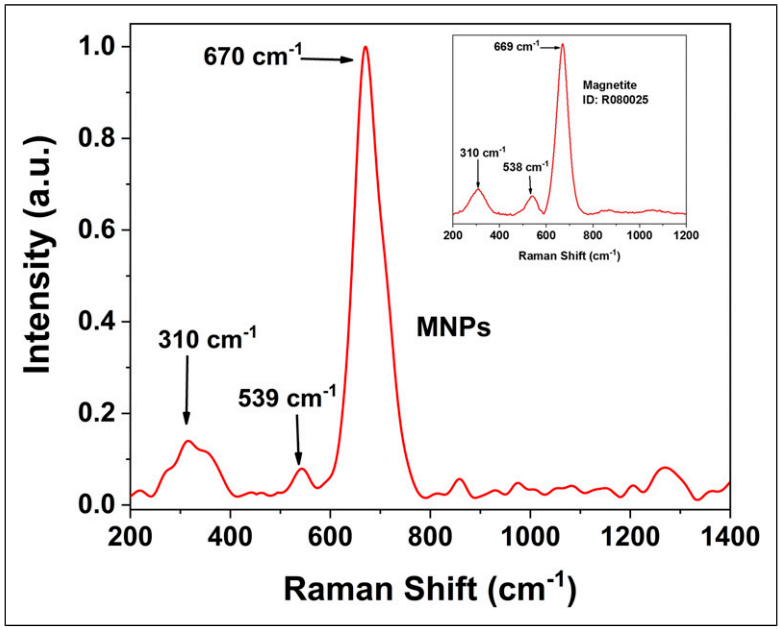

Figure 3. Raman spectrum of synthesized MNPs. The Raman spectrum reported in the "Project RRuFF" database/Code: R080025, is shown in the inset.[62].

315 cm^{-1}, associated with the T_{2g} and E_g transitions, respectively, allows for recognition of other signals attributed to the magnetite phase.[49,52,56] The values obtained in the analysis were compared with the information available in the database Project RRuFF, Code: R080025 for magnetite[57] (inset, Figure 3).

Magnetite, due to its structural characteristic, tends to continue with the oxidative process of Fe^{2+} species, transforming into maghemite.[58,59] Therefore, other regions of the spectrum were analyzed to gather information on the presence of other iron oxides or oxy-hydroxide phases in the sample, such as maghemite or hematite. Special attention is given to the regions 225 and 498 cm^{-1}, which correspond to the $A_{1g}(1)$ and $A_{1g}(2)$ vibrational modes of hematite (Fe_2O_3), respectively. Similarly, the presence of this iron oxide induces at 247 cm^{-1} $E_g(1)$, 291 cm^{-1} $E_g(2)$, 412 $E_g(4)$ and 613 cm^{-1} $E_g(5)$, as reported by Cabrera in his study on coating and characterization of magnetic nanoparticles.[60] On the other hand, Jacintho et al[61] state that the presence of maghemite, the oxidized phase of magnetite with the same crystalline structure (inverse spinel), generates intense signals in the areas at 726, 664 and 350 cm^{-1}. Furthermore, the researchers suggest that the presence of this iron oxide in the analyzed samples results in a prominent peak near 1330 cm^{-1}. Consequently, the absence of these vibrational modes in the Raman spectrum implies either the cessation of the oxidative process of the magnetite nanoparticles or, at very least, that the majority of nanoparticles maintain the magnetite phase.[54,55] Considering the absence of signals associated with other iron oxide phases, such as maghemite and

hematite, and the similarity between the reference spectrum and the spectrum obtained from the analyzed sample, it is suggested that the employed synthesis method is effective for producing the MNPs.

Analysis of the crystal structure of magnetite nanoparticles. X-ray diffraction allows for the study of the crystalline structure of the synthesized nanoparticles, identifying signals attributed to crystallographic planes typical of magnetite. Figure 4 (a) shows the XRD pattern obtained for the synthesized MNPs, which was compared with the reference spectrum from the Crystallography Open Database (COD), ID Code: 2300616, corresponding to magnetite.[62] The signals are observed at the 2θ positions 24.2°, 30.3°, 35.6°, 43.3°, 53.7°, 57.2°, 62.8° and 74.2° which correspond to the crystallographic planes of magnetite with Miller indices (111), (220), (311), (400), (422), (511), (440) and (533)

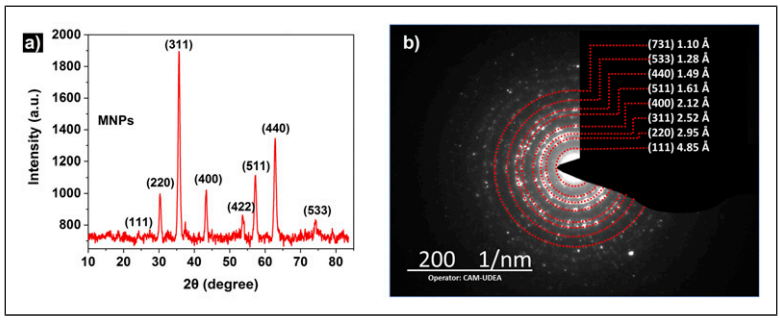

Figure 4. Analysis of the crystal structure of magnetite nanoparticles (a) XRD diffractogram with the corresponding plans indexed; (b) The SAED spectrum shows the main diffraction rings of magnetite.

Table 1. Interplanar distances for crystallographic planes identified by characterization techniques.

Plane	d_{hkl} XRD (Å)	d_{hkl} SAED (Å)	d_{hkl} HR-TEM (Å)	*d_{hkl} reported (Å)
(111)	NF	4.85	NF	4.83
(220)	2.95	2.95	2.97	2.95
(311)	2.52	2.52	2.51	2.52
(400)	2.09	2.12	NF	2.08
(422)	1.71	1.71	NF	1.70
(511)	1.61	1.61	NF	1.60
(440)	1.48	1.49	NF	1.47
(533)	1.28	1.28	1.25	1.27
(731)	NF	1.10	NF	1.09

Note. "*" Values recorded in the crystallography open database, ID Code: 2300616. (NF "No found in characterization analysis").

respectively.[8,54] Additionally, the interplanar distances for each plane were determined using Bragg's law. The obtained values are presented in Table 1. Similarly, using the Scherrer equation and the information provided by the diffractogram for the (311), (440) and (511) planes allowed for the calculation of the average crystallite size, which was found to be 15.1 nm. This value is very similar to the particle size obtained through TEM analysis. Their similarity suggests the presence of single-crystalline phases in the nanoparticles. The lattice parameter was determined to be 8.35 Å, with a unit cell volume of 582.2 $Å^3$, values that are consistent with those reported for magnetite.[62,63] This confirms that both the crystalline arrangement and the interplanar distances, as well as the lattice red of the synthesized nanoparticles, correspond to the inverse spinel structure of magnetite.[22,64] In Figure 4 (b) the Selected Area Electron Diffraction (SAED) pattern is shown, where the discontinuities in the circumference of the concentric rings indicate the presence of a material with a polycrystalline structure.[65,66] Using CrysTBox software,[67] It was possible to index the most intense diffractions present in the SAED pattern, which correspond to the crystallographic planes of the magnetite (111), (220), (311), (400), (511), (440), (533), (731) with their respective interplanar distances as seen in the image (See Table 1).

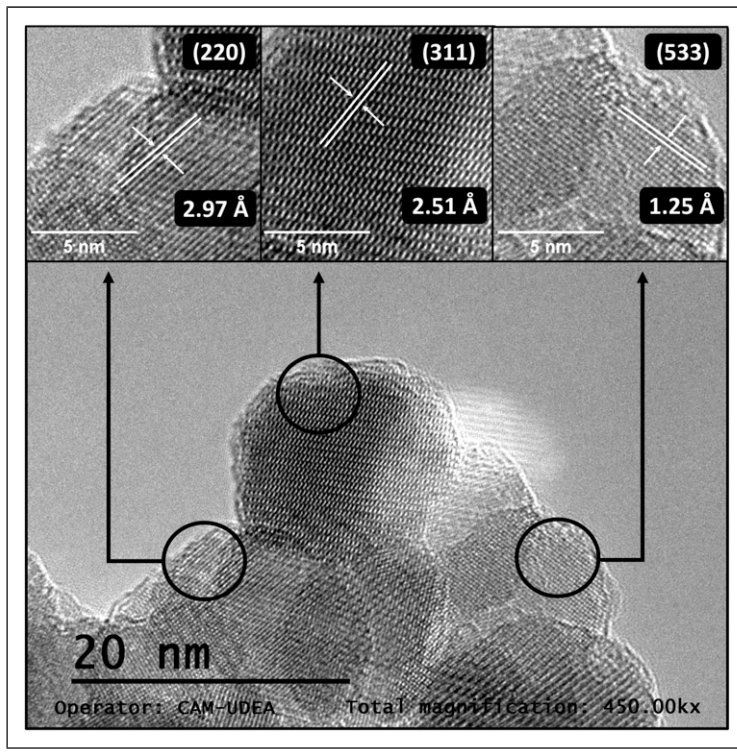

Figure 5. The HR-TEM image shows some lattice fringes on the surface of the NPs. Crystallographic planes are shown in the inset with their respective interplanar distance.

Figure 5 shows HR-TEM images of magnetite nanoparticles. These images allow us to observe several families of crystallographic planes characteristic of the inverse spinel structure of magnetite. The micrographs reveal the main crystallographic plane of the magnetic mineral, the (311) plane, with an interplanar distance of 2.51 Å, a value consistent with that obtained from other analytical methods. Additionally, the boxes in the HR-TEM image clearly show lattice fringes extended through the nanoparticles, as indicated by the solid line. These correspond to the (220) and (533) planes, with interplanar distances of 2.97 and 1.25 Å, respectively.[20,54,68] The crystallographic analysis enabled the identification of the main crystallographic planes associated with the inverse spinel structure of magnetite. The comparison between the XRD pattern, the SAED pattern, and the information provided by the HR-TEM micrographs is consistent with what has been reported in the literature (see Table 1). Furthermore, both the crystallographic and spectroscopic characterization clearly demonstrate the information of the magnetite phase in the synthesized iron oxide, indicating that electrochemical synthesis is an efficient method for obtaining MNPs.

Characterization of PVA fibers and PVA/MNPs nanocomposite fibers

Morphological analysis of PVA and PVA/MNPs. The fibers were obtained by electrospinning PVA solutions (12% m/v) as a control and PVA/MNPs solutions (12% m/v - 10% m/m/MNPs) for 3 hours, resulting in membranes like those shown in Figure 6. The electrospun membranes have diameters ranging from 6.5 to 7.2 cm. The average mass of PVA membranes was 0.1083 g, while for the PVA/MNPs membranes, it was 0.1241 g. The image shows the dark coloration of the fibers with MNPs. These results indicate the incorporation of MNPs into the fibers that constitute the PVA/MNPs membranes.

This section analyzes the morphology of the fibers, as observed in the SEM micrographs of Figure 7(a) and (c). The images reveal a tubular and continuous morphology for both the PVA and PVA/MNPs fibers. Continuous and homogeneous fibers are observed, with no beads, droplets, or defects associated with the electrospinning process.[69] In Figure 7(b) and (d), the quality and homogeneity of the fibers, as well as the diameter of individual fibers, are shown in greater detail. The average diameter for PVA fibers was 183 ± 28 nm, while for PVA/MNPs nanocomposite fibers, it was 227 ± 32 nm, representing a 27% increase in the diameter with the presence of the MNPs. Similar

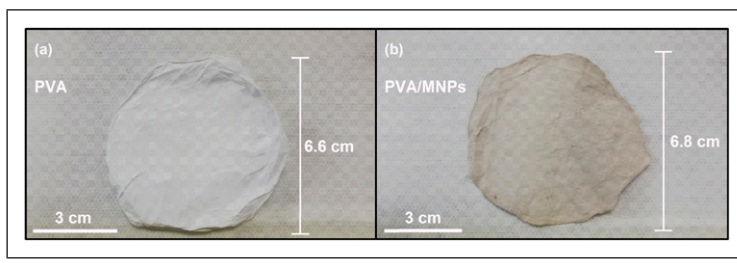

Figure 6. Image of electrospun membranes (a) PVA, (b) PVA/MNPs.

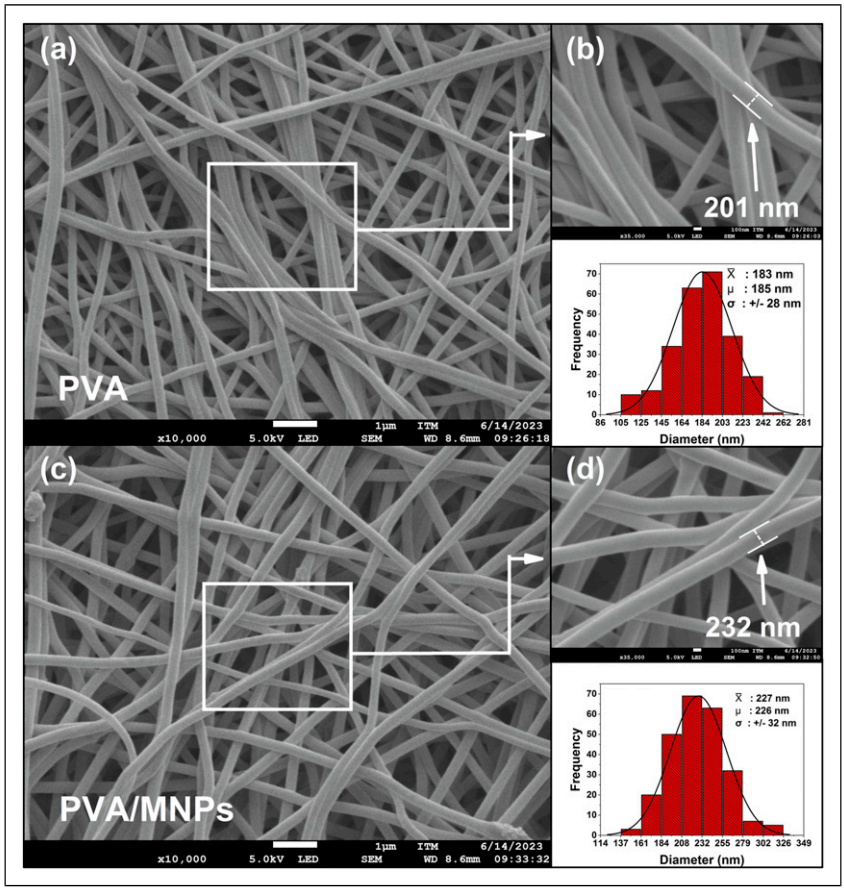

Figure 7. SEM micrograph of (a) PVA & (c) PVA/MNPs fibers at 10.000x. Zoom in of SEM micrographs at 35.000x (b) PVA & (d) PVA/MNPs, with their respective fiber diameter histograms (n = 250, in triplicate).

observations have been reported, showing that the presence of the MNPs increased the fiber radius by 20 to 30%.[70,71] However, other studies have shown that the presence of MNPs leads to a decrease in the diameter of the fibers once the NPs are mixed with the polymer.[72,73] Although the two groups disagree on whether the diameter of the fibers increases or decreases, both agree that this is due to the changes in the rheological and conductive properties of the polymer solution when the MNPs are dispersed. The presence of the MNPs modifies properties such as the conductivity and viscosity, which in turn affect the diameter and morphology of the fibers. Additionally, researchers agree that small variations in atmospheric factors, such as temperature and humidity, also influence the morphological modifications of the fibers.[37,69,74] In the present study, the increase in fiber diameter is attributed to the incorporation of MNPs into the polymeric fibers.

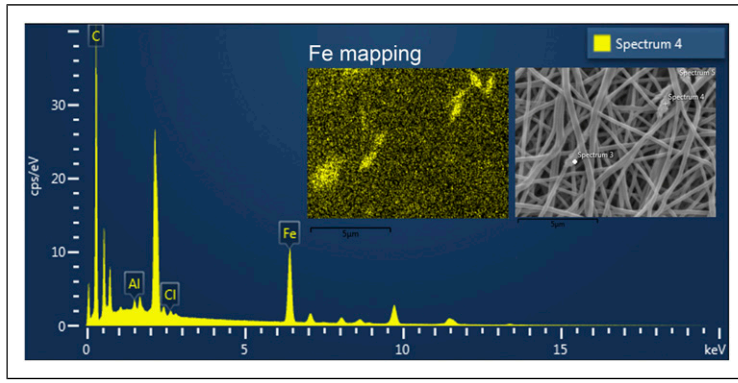

Figure 8. EDS analysis of PVA/MNPs fibers.

Composition analysis of PVA/MNPs nanocomposite fibers. X-ray energy dispersion (EDS) results are shown in Figure 8, where iron and oxygen atoms from Fe_3O_4 are homogeneously distributed on the surface of all the fibers. However, some regions exhibit an agglomeration of MNPs. The presence of these MNPs clusters in the fibers is attributed to the lack of surface modification and the incomplete dispersion of the nanoparticles in the polymer solution.[75] Although the sonication process aids in dispersing the MNPs, they are highly prone to forming agglomerates due to Van der Waals forces and magnetic interactions, leading to the formation of these agglomerates after exposure to dispersion methods.[76] According to the EDS analysis, the surface iron atoms were found to account for 7.3% of the atomic weight in various measured areas, which is consistent with the concentration of MNPs in the PVA solution.

FTIR analysis of PVA and PVA/MNPs nanocomposite fibers was performed to identify the main signals associated with PVA and to evaluate whether significant modifications occurred in the presence of MNPs. Related studies on the development of materials with embedded nanoparticles have reported changes in the signals attributed to the functional groups of polymeric materials once the nanoparticles are integrated into their structure.[8,77] For this reason, the region between 400 and 600 cm^{-1} was excluded, as this range contains signals attributed to Fe-O bond stretches typical of magnetite, rather than signals indicating changes or molecular interactions between the polymer and the oxide.[72,78]

In Figure 9, both spectra show a broad band corresponding to the stretching of alcohol groups (OH) between 3100 and 3500 cm-.[1] Additionally, the band observed between 2900 and 2990 cm^{-1}, corresponding to the vibrational mode of the C-H bonds of the alkyl groups.[45,71,79] In the region close to 1730 cm^{-1}, the vibrational band associated with the carbonyl (C = O) and carbon-oxygen (C-O) bonds of the acetate groups is observed. This indicates that these groups are linked to the molecular structure of the polymer and that the PVA is not completely hydrolyzed.[80] Additionally, signals attributed to bending vibrations of the CH_2 bonds and stretching of the C-O bond are observed in regions 1420, 1240 and 1090 cm^{-1}, corresponding to the secondary alcohols of the PVA structure.[72,81] It is important to highlight that, based on these results, the FTIR spectra of both samples

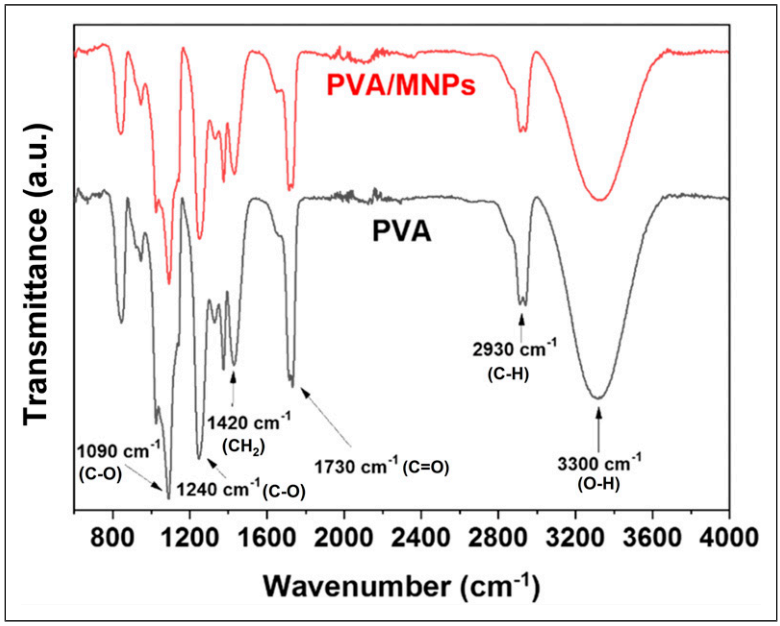

Figure 9. Comparison between FTIR spectra of PVA and PVA/MNPs fibers.

show no significant differences, indicating that the presence of MNPs does not alter the chemical environment of the functional groups in the PVA structure. A characteristic PVA pattern is observed for both materials,[80] further confirming that the presence of MNPs does not affect the chemical structure of the polymer.[72,82]

However, a study conducted on MNPs embedded in PVA/Polyaniline fibers reported a decrease in the elongation band associated with the OH groups of PVA as the concentration of MNPs exceeded 15% w/w. This phenomenon is due to the interaction of the alcohol group with the oxygen atoms in the magnetite, leading to the reduction of this band and the appearance of new ones.[71] Although MNPs can modify the chemical environment of the material, no significant changes to the chemical structure of PVA were observed in the present study, as well as in similar works,[45,70] at concentrations close to 10%.

Magnetic analysis of PVA/MNPs nanocomposite fibers. Magnetic analysis was performed using magnetization measurements (magnetization vs applied magnetic field, MvsH) to determine the saturation magnetization of nanocomposite fibers. Figure 10 presents the MvsH curves for MNPs and PVA/MNPs nanocomposite fibers, where the saturation magnetization (Ms) obtained for magnetic nanoparticles was 79.3 emu/g. This value is consistent with previous studies, which reported magnetization measurements for pure magnetite in the range 92–100 emu/g.[83] The saturation magnetization value for PVA/MNPs nanocomposite fibers was 61.5 emu/g. The reduced magnetization observed in the

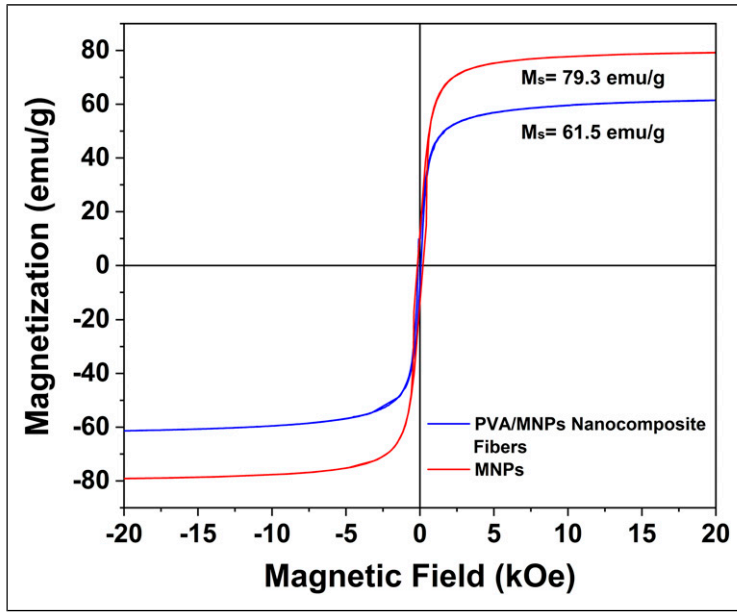

Figure 10. Magnetization curves: Hysteresis measurements for MNPs and PVA/MNPs nanocomposite fibers at 300 k.

PVA/MNPs nanocomposite fibers could be attributed to surface disorder, spin misalignment, or the random alignment of magnetic moments at the particle surface, which results from the surface interaction between magnetite nanoparticles and polyvinyl alcohol polymer.[45,84] However, based on the Ms values displayed by PVA/MNPs nanocomposite fibers, this system shows promise for broad applications, particularly in biomedical fields as a stimuli-responsive an external magnetic field.[10,45,85]

The magnetic properties of the PVA/MNPs membranes presented in this work represent a significant advance in the development of electrospun nanocomposites responsive to magnetic stimuli. This system offers the advantage of remote and non-invasive activation by an external magnetic field, eliminating the need for more complex stimuli such as pH changes, enzymes, exposure to electromagnetic radiation, thermal variations, or electrical pulses.[33,86,87] Furthermore, the high surface-to-volume ratio of electrospun materials presents a clear advantage over smooth films or membranes in applications requiring exposure to a large surface area.[88] In addition, the results demonstrate that the electrospinning technique does not eliminate the magnetic properties of the nanoparticles. Although the magnetic conductivity Ms decreases compared to pure magnetite, the obtained value (61.5 emu/g) falls within the range reported for devices used in magnetically stimulated controlled drug release. Several studies show that incorporating nanoparticles into polymer matrices such as chitosan-agarose, polylactic acid, or PVA allows the production of nanocomposite materials with significant Ms values (50 to 70 emu/g).[45,89,90] While these Ms values are lower than those reported for pure

nanoparticles, they are sufficient to allow an effective response to external magnetic stimuli, thus enabling the modulation of drug release kinetics. Moreover, the ability of PVA/MNPs membranes to respond to DC magnetic field stimuli offers an advantage over hyperthermia-activated drug delivery systems, which require relatively complex equipment and optimized operating conditions to reach temperatures that do not induce drug degradation.[91] These results demonstrate that the processing method used to manufacture PVA/MNPs membranes allows obtaining magnetic nanocomposites whose Ms values are comparable to the values reported for devices for controlled drug delivery by magnetic stimuli, validating the viability of electrospinning as a suitable processing method in the design of potential drug release systems in a controlled, remote and easily activated manner.

Profile release of acetaminophen by diffusion using magnetically responsive PVA/MNPs Membranes. Figure 11 shows the results of the acetaminophen release profile by diffusion, obtained at 5, 30, 60, 90, 120, 150, 180, and 210 minutes at 243 nm from PVA and PVA/MNPs membranes. In Figure 11(a), a schematic representation of the diffusion cell used in the experiments is presented. Figure 11(b) displays box plots illustrating the

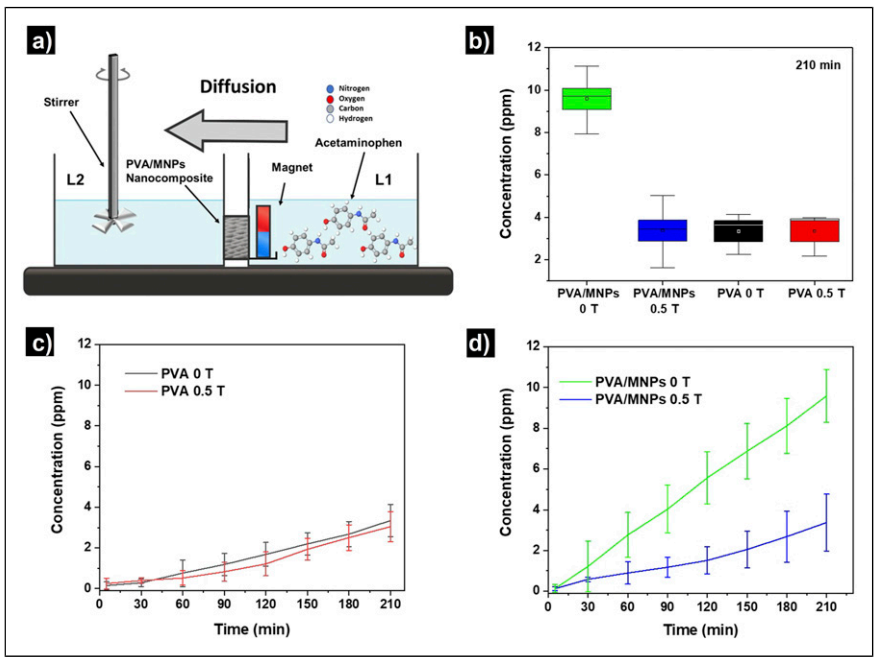

Figure 11. Release profile by diffusion mechanism of PVA and PVA/MNPs membranes. (a) Schematic representation of the diffusion test. (b) Box plots illustrating the distribution of acetaminophen concentrations detected. (c) Release profile of PVA membranes under 0 T and 0.5 T external magnetic fields. (d) Release profile of PVA/MNPs membranes under 0T and 0.5 T external magnetic fields.

distribution of acetaminophen concentrations detected in L2 after the experiment was completed. Notably, the PVA/MNPs-0T membranes show a different release behavior compared to their counterparts subjected to a 0.5 T magnetic field (PVA/MNPs-0.5 T), exhibiting higher concentration values (11.2 and 3.5 ppm, respectively). In contrast, the membranes without MNPs appear to show no significant changes in concentration of acetaminophen, indicating that the presence of the magnetic field has little to no effect on drug release for these membranes (3.2 and 3.3 ppm, respectively). Figure 11(c) shows the release profiles obtained using PVA membranes, both in the presence and absence of a magnetic field. It can be observed that there is no significant difference between membranes exposed to the magnetic field and those that were not, indicating that the drug retention effect cannot be attributed to external magnetic field influence. These results suggest that PVA membranes are not affected by the presence of a magnetic field, consistent with previous reports in similar experimental conditions.[45,46] Based on the experimental data obtained, it is evident that diffusion channels are formed within the membrane, allowing acetaminophen to migrate from a region of higher concentration (L1) to one of lower concentration (L2). However, upon incorporation of MNPs into the PVA fibers, these channels are altered, resulting in an increased diffusion rate of the drug, as shown in Figure 11(d). When the PVA/MNPs fibers are subjected to a magnetic field, the nanoparticles align in the direction of the field, leading to the obstruction of the diffusion channels along the fibers. As a result, the pathway through which the drug diffuses is interrupted.

After considering a possible drug retention mechanism by PVA/MNPs–0.5 T fibers, an important question arises: why in there a clear disparity in drug diffusion behavior between PVA/MNPs–0T membranes and PVA-0T, as illustrated in Figure 11(c) and (d)?.

To explain this phenomenon, we must consider the intermolecular environment present on the surface of both materials (MNPs and PVA) as well as on the surface of the drug, which enables certain van der Waals type interactions. The molecular structure of the polymer includes two main functional groups: the acetate $(C_2H_3O_2)^-$ group and the hydroxyl group $(OH)^-$, the latter being the predominant one.[92] On the other hand, the acetaminophen molecule contains a hydrogen bond to atoms (N and O). According to previous studies, these hydrogens are capable of forming hydrogen bonds with the oxygen atoms in the polymeric chain, which implies an attraction to the polymer structure, thereby affecting the diffusion process of the drug within the PVA membranes.[93,94] In the case of MNPs, the interaction between the oxide surface and the drug has also been reported. However, these Van der Waals type interactions are weaker compared to hat observed with the polymer. For this reason, the functionalization of nanoparticles with carrier agents and their subsequent coating with drugs is a common strategy in biomedical applications.[14] Therefore, it was expected that the diffusion process in the PVA-0T membrane would be slower than in the PVA/MNPs-0T membrane, because in the former, there is a larger exposed surface area available for interaction with the drug, whereas in the latter, this surface is partially obstructed by the presence of nanoparticles.

Statistical analysis was performed to evaluate the influence of the experimental factors involved in drug release, namely the presence of magnetite nanoparticles and exposure to a 0.5 T magnetic field. The study considered the overall behavior of each system (PVA-0T,

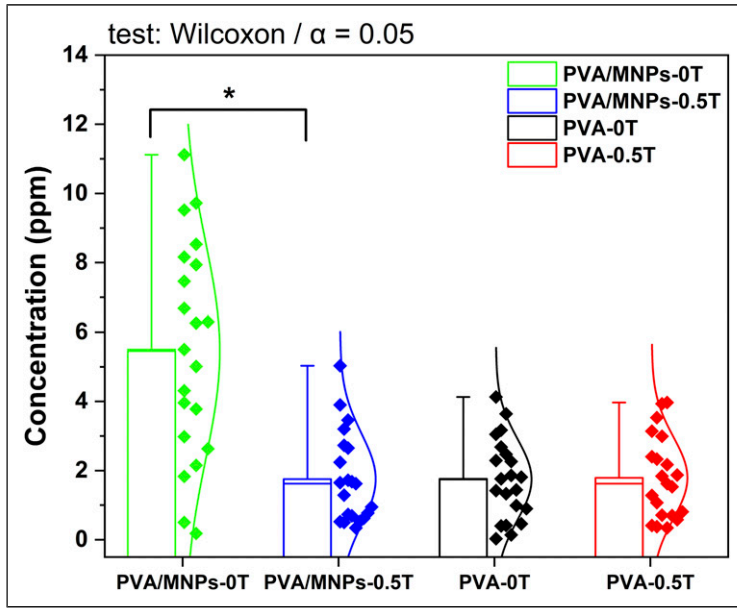

Figure 12. Box and whisker plots show the overall distribution of acetaminophen concentrations for each experimental system. Statistical analyses were performed using the Mann-Whitney U test (Wilcoxon rank-sum test) with a significance level of $\alpha = 0.05$. The asterisk (*) indicates statistically significant differences between the groups compared. Each group includes $n = 21$ measurements corresponding to the complete temporal monitoring of drug release, including repeats.

PVA-0.5 T, PVA/MNPs-0T and PVA/MNPs-0.5 T), represented by the acetaminophen concentration values obtained over the experimental time (see Figure 12). The nonparametric Mann-Whitney U test was performed to assess significant differences between the two groups of interest, "PVA-0T versus PVA-0.T" and "PVA/MNPs-0T versus PVA/MNPs-0.5 T". The test revealed a statistically significant difference between the PVA/MNPs-0T and PVA/MNPs-0.5 T systems, with a p-value = .00015 (W = 371.5). This result supports the observation shown in Figure 11 (d), where the overall concentration values obtained for PVA/MNPs-0T are higher than those recorded for its counterpart. On the other hand, the comparison test performed for pristine PVA membranes indicated that there were no significant differences between the systems, with a reported p-value of 0.94985 (W = 217.5). Therefore, there is sufficient evidence that the acetaminophen release process for MNP-free membranes is not affected by the presence or absence of a magnetic field.

Conclusions

Nanocomposite fibers of PVA/MNPs were obtained via the electrospinning method, exhibiting tubular morphology, homogeneous distribution of nanoparticles, and no

defects associated with the electrospinning process. The MNPs were synthesized using an electrochemical method under nontoxic and sustainable conditions, with NaCl, water and alcohol as the electrolyte solution at room temperature. The results of crystallographic and Raman spectroscopy analyses showed that the synthesized iron oxide nanoparticles contained a magnetite phase. The main signals associated with the crystallographic planes of the magnetic material were identified, along with the signal most representative of the vibrational mode of the magnetite phase. Furthermore, electrochemical synthesis produced nanoparticles with a size of approximately 14 nm, making them ideal for embedding in polymer fibers. In the composition analysis, it was observed that the polymer structure of PVA was not affected by the magnetite nanoparticles. SEM images showed a 27% increase in the diameter of the PVA/MNP fibers once the MNPs were embedded in the polymer matrix. At the same time, the fibers were confirmed to be free of morphological defects such as beads, droplets, discontinuities, or any other defects associated with the manufacture of electrospun fibers. The magnetic behavior of all samples, including magnetite nanoparticles (MNPs) and PVA/MNPs nanocomposite fibers, shows high saturation magnetization values of 79.3 and 61.5 emu/g, respectively. In the PVA/MNPs membranes presented in this work, the magnetite nanoparticles may act as a dynamic barrier, restricting the diffusion of the active component embedded in the matrix in this case, acetaminophen, used as a model drug when an external magnetic field is applied, and facilitating its release in absence of the such a field, as clearly illustrated in the diffusion-based release profile evaluations. These results indicate that the developed nanocomposite membranes hold promise for applications as stimuli-responsive systems. It is important to highlight that one limitation of this study is that the drug release mechanism under dynamic magnetic conditions was evaluated only in a model environment. Further investigation is required to assess the system's performance in more complex or biologically relevant conditions, including in vitro or in vivo settings.

Acknowledgements

The authors thank "Instituto Tecnológico Metropolitano" for support provided by the project.

CRediT authorship contribution

A. Fernandez Data curation, Formal analysis, Investigation, Software, Visualization, Writing – original draft. **T. Marín** Conceptualization, Investigation, Methodology, Project administration, Resources, Supervision, Validation, Writing – review and editing. **O. D. Gutierrez** Conceptualization, Investigation, Resources, Writing – review and editing. **O. Arnache** Conceptualization, Resources, Writing – review and editing.

Declaration of conflicting interests

The authors declared no potential conflicts of interest with respect to the research, authorship, and/or publication of this article.

Funding

The authors disclosed receipt of the following financial support for the research, authorship, and/or publication of this article: Instituto Tecnológico Metropolitano.

ORCID iD

Tiffany Marin https://orcid.org/0000-0002-9409-0638

References

1. Karuthedath Parameswaran A, Azadmanjiri J, Palaniyandy N, et al. Recent progress of nanotechnology in the research framework of all-solid-state batteries. *Nano Energy* 2023; 105: 107994.
2. Singh H and Kaur K. Role of nanotechnology in research fields: medical sciences, military & tribology- A review on recent advancements, grand challenges and perspectives. *Mater Today Proc*. 2023, In press.
3. Srivastava A, Raviya M and Raval H. A novel temperature-responsive mixed matrix ultra-filtration membrane based on boron nitride nanomaterial. *J Thermoplast Compos Mater* 2023; 36: 2412–2434.
4. Chen M, Quan G, Sun Y, et al. Nanoparticles-encapsulated polymeric microneedles for transdermal drug delivery. *J Contr Release* 2020; 325: 163–175.
5. Sell M, Lopes AR, Escudeiro M, et al. Application of nanoparticles in cancer treatment: a concise review. *Nanomaterials* 2023; 13: 2887.
6. Zailan FD, Chen RS, Husein FM, et al. Improved mechanical, magnetic and radiation shielding performance of rubbery polymer magnetic nanocomposites through incorporation of Fe3O4 nanoparticles. *Compos Appl Sci Manuf* 2024; 186: 108385.
7. Akhtar N, Teo Y, Najeeb NM, et al. Synthesis and characterization of magnetic nanostructured lipid carriers (mNLCs) for drug delivery. *Int J Electrochem Sci* 2018; 13: 12040–12048.
8. Ahmed MK, Zayed MA, El-dek SI, et al. Nanofibrous ε-polycaprolactone scaffolds containing Ag-doped magnetite nanoparticles: physicochemical characterization and biological testing for wound dressing applications in vitro and in vivo. *Bioact Mater* 2021; 6: 2070–2088.
9. Vandghanooni S, Sanaat Z, Barar J, et al. Recent advances in aptamer-based nanosystems and microfluidics devices for the detection of ovarian cancer biomarkers. *TrAC, Trends Anal Chem* 2021; 143: 116343.
10. Marín T, Montoya P, Arnache O, et al. Bioactive films of zein/magnetite magnetically stimuli-responsive for controlled drug release. *J Magn Magn Mater* 2018; 458: 355–364.
11. Leganés J, Rodríguez AM, Arranz MA, et al. Magnetically responsive hydrophobic pockets for on–off drug release. *Mater Today Chem* 2022; 23: 100702.
12. Zimina T, Sitkov N, Brusina K, et al. Magnetically controlled transport of nanoparticles in solid tumor tissues and porous media using a tumor-on-a-chip format. *Nanomaterials* 2024; 14: 2030.
13. Materón EM, Miyazaki CM, Carr O, et al. Magnetic nanoparticles in biomedical applications: a review. *Appl Surf Sci Adv* 2021; 6: 100163.
14. Yang Y, Liu Y, Song L, et al. Iron oxide nanoparticle-based nanocomposites in biomedical application. *Trends Biotechnol*. 2023; 41: 1471–1487.

15. Kaur S, Singh M, Brkljaca R, et al. Artificial magnetosomes: molecularly restructured SPIONs with enhanced potential for magnetic imaging. *Mater Today Chem* 2024; 40: 102206.
16. Dejene BK. Eco-friendly synthesis of metallic nanoparticles from agri-food waste extracts: applications in food packaging and healthcare–A critical review. *Mater Today Chem* 2025; 45: 102619.
17. Graham W, Torbett-Dougherty M, Islam A, et al. Magnetic nanoparticles and drug delivery systems for anti-cancer applications: a review. *Nanomaterials* 2025; 15: 285.
18. Sharma PK, Dorlikar S, Rawat P, et al. 1 - Nanotechnology and its application: a review. In: Khondakar KR and Kaushik AK (eds). *Nanotechnology in Cancer Management*. Elsevier, pp. 1–33.
19. Chaabane L, Chahdoura H, Mehdaoui R, et al. Functionalization of developed bacterial cellulose with magnetite nanoparticles for nanobiotechnology and nanomedicine applications. *Carbohydr Polym* 2020; 247: 116707.
20. Rizk HE and El-Hefny NE. Synthesis and characterization of magnetite nanoparticles from polyol medium for sorption and selective separation of Pd(II) from aqueous solution. *J Alloys Compd* 2020; 812: 152041.
21. Fajaroh F, Setyawan H, Widiyastuti W, et al. Synthesis of magnetite nanoparticles by surfactant-free electrochemical method in an aqueous system. *Adv Powder Technol* 2012; 23: 328–333.
22. Niculescu AG, Chircov C and Grumezescu AM. Magnetite nanoparticles: synthesis methods – a comparative review. *Methods* 2022; 199: 16–27.
23. Ledesma-Fosados LI, Gallardo-Rivas NV, Páramo-García U, et al. Enhanced control of magnetite nanoparticle electrosynthesis through cyclic voltammetry. *Int J Electrochem Sci* 2025; 20: 100956.
24. Marín T, Ortega D, Montoya P, et al. A new contribution to the study of the electrosynthesis of magnetic nanoparticles the influence of the supporting electrolyte. *J Appl Electrochem*. 2014; 44: 1401–1410.
25. Setyawan H and Widiyastuti W. Progress in the preparation of magnetite nanoparticles through the electrochemical method. *KONA Powder and Particle Journal* 2019; 36: 145–155.
26. Hajiyeva FV, Shirinova HA, Jafarov MA, et al. Effect of magnetite nanoparticles on the structure, thermal and magnetic properties of the high-density polyethylene. *J Thermoplast Compos Mater*. 2026; 39: 82–101.
27. Anushree C, Rahim FA, Vanithakumari SC, et al. Electrospun superparamagnetic fibrous composite nanofiber films for enhanced oil spill recovery: effect of capping and magnetic nanoparticle loading on oil sorption efficiency. *Compos Appl Sci Manuf* 2023; 171: 107591.
28. Molina BG, Enshai H, Gil A, et al. Electroactive self-standing polyester membranes prepared using magnetite/poly(3,4-ethylenedioxythiophene) core-shell particles. *Polymer* 2024; 311: 127535.
29. Li H, Wu C, Yu X, et al. Recent advances of PVA-based hydrogels in cartilage repair application. *J Mater Res Technol* 2023; 24: 2279–2298.
30. Wang S, Wang C, Zhang B, et al. Preparation of Fe3O4/PVA nanofibers via combining in-situ composite with electrospinning. *Mater Lett* 2010; 64: 9–11.
31. Chen Y and Hou S. Application of magnetic nanoparticles in cell therapy. *Stem Cell Res Ther* 2022; 13: 135.

32. Elsherbini AM and Sabra SA. Nanoparticles-in-nanofibers composites: emphasis on some recent biomedical applications. *J Contr Release* 2022; 348: 57–83.
33. Fu Y, Wei Z, Wan Z, et al. Recent process of multimode stimuli-responsive flexible composites based on magnetic particles filled polymers: characteristics, mechanism and applications. *Compos Appl Sci Manuf* 2022; 163: 107215.
34. Panda PK, Dash P, Biswal AK, et al. Synthesis and characterization of modified poly(vinyl alcohol) membrane and study of its enhanced water-induced shape-memory behavior. *J Polym Environ* 2022; 30: 3409–3419.
35. Jiang S, Liu S and Feng W. PVA hydrogel properties for biomedical application. *J Mech Behav Biomed Mater* 2011; 4: 1228–1233.
36. Baykara D, Pilavci E, Cesur S, et al. Controlled release of gentamicin from electrospun Poly(Vinyl Alcohol)/Gelatin nanofibers: the effect of crosslinking time using glutaraldehyde vapor. *ChemistrySelect* 2023; 8: e202203681.
37. Al-Abduljabbar A and Farooq I. Electrospun polymer nanofibers: processing, properties, and applications. *Polymers* 2023; 15: 65.
38. Amna T and Hassan MS. Nanofibers and nanotextured materials: design insights, bactericidal mechanisms and environmental advances. *Nanomaterials* 2023; 13: 2891.
39. Funnell JL, Ziemba AM, Nowak JF, et al. Assessing the combination of magnetic field stimulation, iron oxide nanoparticles, and aligned electrospun fibers for promoting neurite outgrowth from dorsal root ganglia in vitro. *Acta Biomater* 2021; 131: 302–313.
40. Serrano-Aroca Á, Cano-Vicent A, Sabater I, et al. Scaffolds in the microbial resistant era: fabrication, materials, properties and tissue engineering applications. *Mater Today Bio* 2022; 16: 100412.
41. Torres-Martinez EJ, Bravo JMC, Medina AS, et al. A summary of electrospun nanofibers as drug delivery system: drugs loaded and biopolymers used as matrices. *Curr Drug Deliv* 2018; 15: 1360–1374.
42. Ebadi M, Buskaran K, Bullo S, et al. Drug delivery system based on magnetic iron oxide nanoparticles coated with (polyvinyl alcohol-zinc/aluminium-layered double hydroxide-sorafenib). *Alex Eng J* 2021; 60: 733–747.
43. Burke L, Mortimer CJ, Curtis DJ, et al. In-situ synthesis of magnetic iron-oxide nanoparticle-nanofibre composites using electrospinning. *Mater Sci Eng C* 2017; 70: 512–519.
44. Cai N, Li C, Han C, et al. Tailoring mechanical and antibacterial properties of chitosan/gelatin nanofiber membranes with Fe3O4 nanoparticles for potential wound dressing application. *Appl Surf Sci* 2016; 369: 492–500.
45. Perera AS, Zhang S, Homer-Vanniasinkam S, et al. Polymer–magnetic composite fibers for remote-controlled drug release. *ACS Appl Mater Interfaces* 2018; 10: 15524–15531.
46. Sivasankarapillai VS, Das SS, Sabir F, et al. Progress in natural polymer engineered biomaterials for transdermal drug delivery systems. *Mater Today Chem* 2021; 19: 100382.
47. Shi K, Nokhodchi A and Ghafourian T. Magnetic microscale polymeric nanocomposites in drug delivery: advances and challenges. *Drug Discov Today* 2025; 30: 104276.
48. Cabrera L, Gutierrez S, Menendez N, et al. Magnetite nanoparticles: electrochemical synthesis and characterization. *Electrochim Acta* 2008; 53: 3436–3441.

49. Montoya P, Marín T, Mejía S, et al. Elucidation of the mechanism of electrochemical formation of magnetite nanoparticles by in Situ Raman spectroscopy. *J Electrochem Soc* 2017; 164: D1056–D1065.
50. Mohammed L, Gomaa HG, Ragab D, et al. Magnetic nanoparticles for environmental and biomedical applications: a review. *Particuology* 2017; 30: 1–14.
51. Mohammad F and Yusof NA. Surface ligand influenced free radical protection of superparamagnetic iron oxide nanoparticles (SPIONs) toward H9c2 cardiac cells. *J Mater Sci* 2014; 49: 6290–6301.
52. Shebanova ON and Lazor P. Raman spectroscopic study of magnetite (FeFe2O4): a new assignment for the vibrational spectrum. *J Solid State Chem* 2003; 174: 424–430.
53. Galeas Hurtado SG, Alvear Ortiz FD, Guerrero Barragán VH, et al. Síntesis y Caracterización de Nanopartículas de Magnetita. *Revista Politécnica* 2017; 39: 61–66.
54. Qu XF, Yao QZ, Zhou GT, et al. Formation of hollow magnetite microspheres and their evolution into durian-like architectures. *J Phys Chem C* 2010; 114: 8734–8740.
55. Slavov L, Abrashev MV, Merodiiska T, et al. Raman spectroscopy investigation of magnetite nanoparticles in ferrofluids. *J Magn Magn Mater* 2010; 322: 1904–1911.
56. Testa-Anta M, Ramos-Docampo MA, Comesaña-Hermo M, et al. Raman spectroscopy to unravel the magnetic properties of iron oxide nanocrystals for bio-related applications. *Nanoscale Adv* 2019; 1: 2086–2103.
57. Lafuente B, Downs RT, Yang H, et al. 1. The power of databases: the RRUFF project. In: Armbruster T and Danisi RM (eds). *Highlights in Mineralogical Crystallography*. De Gruyter (O), pp. 1–30.
58. Cornell RM and Schwertmann U. *The iron oxides: structure, properties, reactions, occurrences and uses*. 2nd edition. Wiley VCH, 2003.
59. Mücke A and Raphael Cabral A. Redox and nonredox reactions of magnetite and hematite in rocks. *Geochemistry* 2005; 65: 271–278.
60. Cabrera Salazar JV. *Síntesis de nanopartículas de Fe3O4 (magnetita) y su recubrimiento usando carbonización de glucosa mediante un proceso solvotérmico*. [Master Thesis]. Instituto Potosino de Investigacion Científica y Tecnológica, A.C, 2017. https://repositorio.ipicyt.edu.mx///handle/11627/3105 (accessed 17 September 2023).
61. Jacintho GVM, Corio P and Rubim JC. Surface-enhanced raman spectra of magnetic nanoparticles adsorbed on a silver electrode. *J Electroanal Chem* 2007; 603: 27–34.
62. Vaitkus A, Merkys A and Gražulis S. Validation of the crystallography open database using the crystallographic information framework. *J Appl Cryst* 2021; 54: 661–672.
63. Rodríguez-López A, Paredes-Arroyo A, Mojica-Gomez J, et al. Electrochemical synthesis of magnetite and maghemite nanoparticles using dissymmetric potential pulses. *J Nanopart Res* 2012; 14: 993.
64. Ovejero JG, Mayoral A, Cañete M, et al. Electrochemical synthesis and magnetic properties of MFe2O4 (M = Fe, Mn, Co, Ni) nanoparticles for potential biomedical applications. *J Nanosci Nanotechnol* 2019; 19: 2008–2015.
65. Roca AG. *Preparación de Nanopartículas Magnéticas Uniformes y de Alta Cristalinidad para Biomedicina*. [PhD Thesis]. Universidad Complutense de Madrid, 2010. https://digital.csic.es/handle/10261/22726 (accessed 7 April 2023).

66. Xiong Z, Sun ZB, Zheng ML, et al. A facile method for the room-temperature synthesis of water-soluble magnetic Fe3O4 nanoparticles: combination of in situ synthesis and decomposition of polymer hydrogel. *Mater Chem Phys* 2011; 130: 72–78.
67. Klinger M and Jäger A. It crystallographic tool box (ıt CrysTBox): automated tools for transmission electron microscopists and crystallographers. *J Appl Crystallogr* 2015; 48: 2012–2018.
68. Baños JGC, Lara VEN and Puentes CO. Magnetita (Fe3O4): una estructura inorgánica con múltiples aplicaciones en catálisis heterogénea. *Rev Colomb Quím* 2017; 46: 42–59.
69. Bhardwaj N and Kundu SC. Electrospinning: a fascinating fiber fabrication technique. *Biotechnol Adv* 2010; 28: 325–347.
70. Ger T-R, Huang H-T, Huang C-Y, et al. Study of polyvinyl alcohol nanofibrous membrane by electrospinning as a magnetic nanoparticle delivery approach. *J Appl Phys* 2014; 115: 17B908.
71. Ibrahim Takai Z, Kamarulzaki Mustafa M, Ahmad Sekak K, et al. Fabrication, characterization and X-band microwave absorption properties of PAni/Fe3O4/PVA nanofiber composites materials. *Arab J Chem* 2020; 13: 7978–7989.
72. Jannah M, Taufiq A, Hidayat N, et al. Preparation and structural characterization of Nanosized PVA/Fe 3 O 4 fibers. *J Phys Conf* 2018; 1093: 012040.
73. Durán Guerrero JG. *Desarrollo de materiales híbridos nanoestructurados basados en nanofibras de CMC/PVA y nanopartículas de magnetita*. [Masters]. Universidad Autónoma de Nuevo León, 2017. https://eprints.uanl.mx/17872/ (accessed 26 June 2023).
74. Baig N, Kammakakam I and Falath W. Nanomaterials: a review of synthesis methods, properties, recent progress, and challenges. *Mater Adv* 2021; 2: 1821–1871.
75. Karbowniczek JE, Ura DP and Stachewicz U. Nanoparticles distribution and agglomeration analysis in electrospun fiber based composites for desired mechanical performance of poly(3-hydroxybuty-rate-co-3-hydroxyvalerate (PHBV)) scaffolds with hydroxyapatite (HA) and titanium dioxide (TiO2) towards medical applications. *Compos B Eng* 2022; 241: 110011.
76. Vikesland P J, Rebodos R L, Bottero J Y, et al. Aggregation and sedimentation of magnetite nanoparticle clusters. *Environ Sci Nano* 2016; 3: 567–577.
77. Aktürk A, Erol Taygun M, Karbancıoğlu Güler F, et al. Fabrication of antibacterial polyvinylalcohol nanocomposite mats with soluble starch coated silver nanoparticles. *Colloids Surf A Physicochem Eng Asp* 2019; 562: 255–262.
78. Chen X, Zhou Y, Han H, et al. Optical and magnetic properties of small-size core–shell Fe3O4@C nanoparticles. *Mater Today Chem* 2021; 22: 100556.
79. Melo PEF, Oliveira da Silva A, Miranda KWE, et al. Chitosan and polyvinyl alcohol nanocomposite incorporated with carbon dots: a proposal for packaging. *Polymer* 2025; 334: 128755.
80. Mansur HS, Sadahira CM, Souza AN, et al. FTIR spectroscopy characterization of poly (vinyl alcohol) hydrogel with different hydrolysis degree and chemically crosslinked with glutaraldehyde. *Mater Sci Eng C* 2008; 28: 539–548.
81. Ramirez A, Benítez JL, Rojas de Astudillo L, et al. Polymers materials type hydrogels: review of their characterization by ftir, dsc, sem and tem. *Revista Latinoamericana de Metalurgia y Materiales* 2016; 36: 108–130.
82. Alruwaili A, Abdelhaleem S, Tawfik E, et al. Structural, thermal, optical, and ion beam analysis of PVA/CNT polymeric nanocomposite films. *J Thermoplast Compos Mater*. 2025, In press.

83. Mohammad-Beigi H, Yaghmaei S, Roostaazad R, et al. Effect of pH, citrate treatment and silane-coupling agent concentration on the magnetic, structural and surface properties of functionalized silica-coated iron oxide nanocomposite particles. *Phys E Low-dimens Syst Nanostruct* 2011; 44: 618–627.
84. Qureshi AA, Javed S, Javed HMA, et al. Systematic investigation of structural, morphological, thermal, optoelectronic, and magnetic properties of high-purity hematite/magnetite nanoparticles for optoelectronics. *Nanomaterials* 2022; 12: 1635.
85. Jayakrishnan P, Jithin K, Meera K, et al. Synthesis, characterization, magnetoelectric properties and gas sensing application of poly(anthranilic acid-co-indole)/magnetite nanocomposites. *J Thermoplast Compos Mater* 2023; 36: 2523–2542.
86. Li F, Qin Y, Lee J, et al. Stimuli-responsive nano-assemblies for remotely controlled drug delivery. *J Contr Release* 2020; 322: 566–592.
87. Ziegler R, Ilyas S, Mathur S, et al. Remote-controlled activation of the release through drug-loaded magnetic electrospun fibers. *Fibers* 2024; 12: 48.
88. Chinnappan BA, Krishnaswamy M, Xu H, et al. Electrospinning of biomedical nanofibers/nanomembranes: effects of process parameters. *Polymers* 2022; 14: 3719.
89. Viteri A, Espanol M, Ginebra M-P, et al. Tailoring drug release from skin-like chitosan-agarose biopolymer hydrogels containing Fe3O4 nanoparticles using magnetic fields. *Chem Eng J* 2025; 517: 164214.
90. Barbosa Mariana Martines de Melo, Oliveira Campos França de Juliene, Dos Santos Lima Quezia, et al. Tailoring the properties of Magnetite/PLA nanocomposites: a composition-dependent study. *Polymers*. 2025; 17: 1713.
91. Phung DC, Nguyen HT, Phuong Tran TT, et al. Combined hyperthermia and chemotherapy as a synergistic anticancer treatment. *J Pharm Investig* 2019; 49: 519–526.
92. Hulupi M and Haryadi H. Synthesis and characterization of electrospinning PVA nanofiber-crosslinked by glutaraldehyde. *Mater Today Proc* 2019; 13: 199–204.
93. Wen H, Morris KR and Park K. Hydrogen bonding interactions between adsorbed polymer molecules and crystal surface of acetaminophen. *J Colloid Interface Sci* 2005; 290: 325–335.
94. Wen Hong, Morris Kenneth R. and Park Kinam. Synergic effects of polymeric additives on dissolution and crystallization of acetaminophen. *Pharm Res*. 2008; 25: 349–358.